Faraday Discussions

Quantum resonances and roaming dynamics in formaldehyde photodissociation

Journal:	*Faraday Discussions*
Manuscript ID	FD-ART-02-2022-000050.R1
Article Type:	Paper
Date Submitted by the Author:	23-Mar-2022
Complete List of Authors:	Foley, Casey; University of Missouri Columbia College of Arts and Science, Chemistry Xie, Changjian; University of New Mexico College of Arts and Sciences Guo, Hua; University of New Mexico College of Arts and Sciences Suits, Arthur; University of Missouri Columbia College of Arts and Science, Chemistry

ARTICLE

Quantum resonances and roaming dynamics in formaldehyde photodissociation

Received 00th January 20xx,
Accepted 00th January 20xx

DOI: 10.1039/x0xx00000x

Casey D. Foley, †,[a] Changjian Xie [b,c,*] Hua Guo[c] and Arthur G. Suits [a,*]

The unimolecular dissociation of formaldehyde is studied via excitation to the $\tilde{A}$ band at several excitation energies from just below the ground state radical dissociation threshold to 5000 cm^{-1} above it. CO product rotational distributions, photofragment excitation spectroscopy and state-correlated slice imaging results are combined with quasiclassical trajectory calculations to reveal manifestions of quantum effects in this complex dissociation process involving interactions among radical, molecular, and roaming pathways. Evidence of nodal structure at the tight transition state to molecular products is investigated and correlations between the CO rotational and H_2 vibrational distributions are used to suggest the transition state modes that are responsible. A large modulation of the roaming yield previously identified and associated to roaming resonances at the onset of the H+HCO(v_1, v_2, v_3=0, 0, 0) product channel suggests a similar origin for enhanced roaming and a roaming yield that is strongly dependent on parent rotation on the $2^6 4^1$ band just 15 cm^{-1} above the H+HCO(0, 2, 1) threshold. Similar resonances are predicted on other bands that share near coincident energies with HCO product vibrational thresholds.

Introduction

Formaldehyde has long served as one of the most revealing systems for the study of unimolecular reaction dynamics,[1] and recent results show we still have a great deal to learn from this remarkable molecule.[2-4] Many factors contribute to its special virtues but foremost among these is the fact that one can prepare single rotational levels on many vibrational bands in the metastable first excited state (S_1), and these dissociate to products H_2 + CO or H + HCO following slow electronic relaxation to the ground state (S_0) or to the triplet state (T_1). All of these products can be detected in single quantum states, with laser-induced fluorescence detection of CO and HCO exploited in much of the early work,[5-10] followed by velocity map imaging (VMI) detection of CO, H_2, and H more recently.[2, 11-15] The extraordinary velocity resolution of VMI then permits fully state-correlated measurements that afford unmatched insight into the dynamical behaviour of this tetra-atomic system undergoing unimolecular decay. Coupled to this has been ever-growing accuracy of the potential energy surfaces (PESs) used to model the dynamics[16-19] and powerful and revealing quasi-classical trajectory (QCT) calculations on these PESs.[2, 15, 20, 21]

The unusual characteristics of these PESs, illustrated in Fig. 1, have also contributed to the special place formaldehyde holds in the dynamics pantheon. The origin of S_1 is just below the high barrier on the ground state that leads to H_2 + CO. Tunnelling dynamics through this barrier has been studied by Stark level crossing spectra revealing a "lumpy continuum" there that we will examine further below.[5, 6] Internal conversion to the ground state is in the weak coupling limit: although there is a conical intersection (CI) between S_1 and S_0, the minimum energy crossing (MEX) is high in energy, and the barrier on S_1 from the Franck-Condon region to the MEX is higher still.[18, 19, 22-24] The possible role of this CI will also be explored in our investigation that follows. On the S_0 state, the radical dissociation threshold is ~3500 cm^{-1} above the tight transition state (t-TS) to molecular products, and this closely coincides with the $2^1 4^3$ vibrational band in S_1. Studies of the CO rotational distributions at the radical threshold and above showed the expected high rotational levels associated with dissociation over the t-TS, but in addition there was a low j_{CO} component not seen below the radical threshold.[8] State-correlated imaging combined with QCT calculations then demonstrated clearly that these low CO rotational levels were formed in coincidence with highly vibrationally excited H_2 as a result of the intramolecular H+HCO reaction at long range.[11, 12] This was ascribed to H atom "roaming" to 3-5 Å, and a "third way" for unimolecular decomposition, roaming, was identified, in addition to barrierless and activated dissociation. The study of roaming has driven an ongoing resurgence of interest in formaldehyde,[2-4] but roaming has been identified in many other systems as well and it is now regarded as common aspect of unimolecular – and even bimolecular – reaction dynamics.[25-27] Roaming also remains a topic of keen theoretical interest as efforts are made

[a] Department of Chemistry, University of Missouri, Columbia MO 65211 USA
[b] Institute of Modern Physics, Shaanxi Key Laboratory for Theoretical Physics Frontiers, Northwest University, Xian, Shaanxi 710127, China
[c] Department of Chemistry and Chemical Biology, University of New Mexico, Albuquerque, New Mexico 87131, USA
† Current address: Combustion Research Facility, Sandia National Laboratories, Livermore, CA 94551 USA
* xcjscu@126.com, *suitsa@missouri.edu
Electronic Supplementary Information (ESI) available: [details of any supplementary information available should be included here]. See DOI: 10.1039/x0xx00000x

to rationalize roaming dynamics in terms of transition state theory or dynamical systems.[28-31]

Aside from our recent report,[4] which we extend in the present work, roaming in formaldehyde has always been treated classically and no evidence of quantum effects has been seen in roaming systems despite the likely quantum nature of a slowly roaming H atom.[32] In detailed studies of the complete CO rotational state and translational energy distributions (TEDs) as a function of the parent H_2CO rotational level, we recently showed that the roaming fraction of the total yield of molecular products exhibited a sharp increase over a very narrow energy range. These effects were not reproduced in QCT, but consistent with quantum dynamics studies in reduced dimensionality, described below, suggesting an orbiting resonance associated with the opening of the H+HCO(K_a=1, ν_1, ν_2, ν_3=0,0,0) channel. That work focused exclusively on dissociation via the lowest rotational levels of the 2^14^3 band at the onset of the radical channel, the origin of which is just 12 cm^{-1} above the H+HCO(0,0,0) asymptote. Here we extend this exploration of quantum dynamics in formaldehyde roaming, looking first at underlying resonances coupling S_1 to S_0, then turning to dissociation from specific rotational levels on several higher S_1 vibrational bands, comparing QCT estimates of roaming yield with experimental measurements on j_{CO}=28, a particular product state that generally shows both roaming and t-TS pathways as distinct features. We find evidence of an additional resonance impacting specific rotational levels of the 2^64^1 band that gives rise to enhanced roaming for j_{CO}=28 and interesting energy dependence over a narrow energy range. We ascribe this to the presence of the H+HCO(0,2,1) threshold just 15 cm^{-1} below the 2^64^1 origin. This in turn leads us to predict enhanced roaming on selected rovibrational levels that exhibit similar near-coincidence with the limited number of low-lying bound states of the HCO product.

Experimental methods

H_2CO monomers were produced by a method adapted from previous experiments in which monomers are liberated from paraformaldehyde upon heating.[9, 33] Paraformaldehyde, anhydrous $MgSO_4$, and glass wool were packed into a KF elbow before the valve. The KF elbow, valve, and connecting stainless steel parts were wrapped with heating cord and heated to ~70°C to liberate H_2CO monomers from paraformaldehyde. A 930 Torr helium backing pressure resulted in a ~5% formaldehyde concentration and a beam temperature of between 10 and 20 K. Beam temperature was estimated from relative populations of H_2CO rovibrational lines and could be adjusted by changing the backing pressure and the valve timing, allowing for an earlier part of the supersonic expansion to be sampled.

UV light was generated by frequency doubled or tripled narrow linewidth (0.1 cm^{-1}) dye lasers pumped by Nd:YAG lasers. Both pump and probe energies were less than 0.2 mJ/pulse. Photofragment excitation (PHOFEX) spectra were obtained by scanning the excitation/dissociation laser from 29460 to 35160 cm^{-1} using resonance-enhanced multiphoton ionization (REMPI) detection of various j_{CO} levels via 2-photon REMPI on the Q($B^1\Sigma^+ \leftarrow X^1\Sigma^+$) transition around 230 nm or H atoms via 2+1 REMPI via $2s(^2S_{1/2}) \leftarrow 1s(^2S_{1/2})$ near 243 nm. Vibrational bands on S_1 covered in this scan range include 2^14^1, 2^16^1, 2^14^3, 2^24^1, 2^24^3, 2^15^1, and 2^64^1 and for the latter we follow the tentative assignment given by Quinn et al.[34] Spectral simulations and were done using PGOPHER[35] and a fit was performed to assign rotational structure in the vibrational bands of the experimental spectra.

For the 2^14^1, 2^14^3, and 2^24^3 vibrational bands, CO REMPI spectra were obtained by fixing the excitation/dissociation laser on a particular parent rovibrational line and scanning the probe laser from 43455 to 43506 cm^{-1}, covering j_{CO} = 0 to 63 for CO (v=0). Accessed H_2CO ground and excited state rotational levels ranged between J=0 and 4, with a rotational energy typically around 6 cm^{-1} and up to 43 cm^{-1}. DC sliced[36] VMI[37, 38] of various j_{CO} levels was also performed following excitation and dissociation of parent rovibrational lines. PHOFEX spectra and images are presented in supplementary information, except that 2^14^3 images were presented in the Supplementary Material for reference 4.

Computational methods

QCT calculations were carried out on the latest S_0 PES of Wang et al.[17] Several initial conditions have been used to explore various dynamics issues. In most calculations, trajectories were initiated at the S_0 equilibrium geometry of H_2CO, with random momenta to match the total energy determined by the S_1 band. This choice of initial conditions is based on the premise that the roaming is ergodic on S_0, thus independent of the initial conditions. To explore the effect of vibrational excitations at the t-TS, initial conditions have been chosen to start the trajectories at the turning points of a specific vibrational level at the saddle point. In addition, trajectories have also been initiated at the MEX between S_0 and S_1, as determined by the recent ab initio calculations,[18, 19] with momenta along the ***h*** and ***g*** vectors spanning the CI branching space. The trajectories were propagated with a time step of 0.05 fs, and terminated when the separation of the products is beyond 20 Å. In the molecular channel, the rovibrational states of the products (H_2 and CO) are determined from the rotational angular momenta and the vibrational energies, which are binned to integer quantum numbers. The QCT calculations were carried out using the VENUS code.[39]

Results and discussion

It will be useful first to review the spectroscopy of formaldehyde on the $\tilde{A}$ band as we will be carefully examining the photochemical behaviour of individual rotational levels.[40] The ground S_0 state has A_1 electronic symmetry while S_1 has A_2. This transition is thus nominally forbidden but allowed via vibronic interactions involving either out-of-plane (b_1 symmetry) or in-plane (b_2 symmetry) vibrations. This yields bands that are either B-type or C-type depending on whether the coupling mode is ν_4, out-of-plane bend, or ν_5/ν_6, asymmetric stretch/wag. Internal conversion from S_1

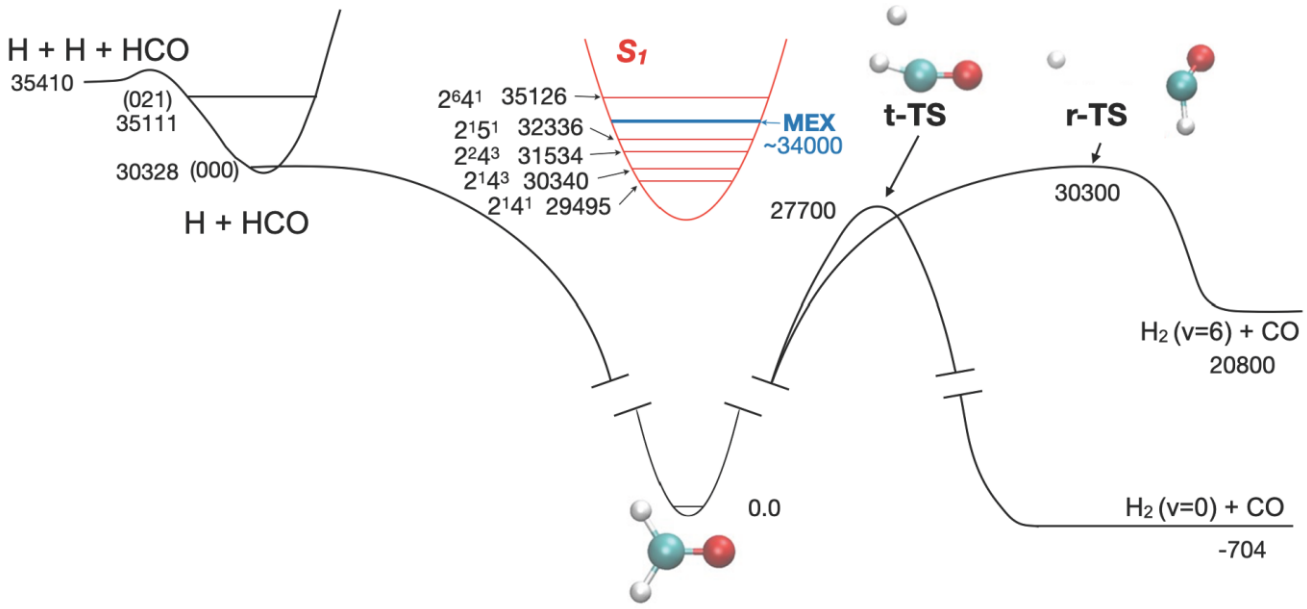

Figure 1. Schematic potential diagram for formaldehyde showing molecular, roaming and radical dissociation pathways. Origins for S_1 vibrational bands examined here are indicated, as are two near-resonant HCO product levels. Structures of the tight-Transition state (t-TS) and roaming transition state (r-TS) are shown. MEX: minimum energy S_1/S_0 crossing. Energies in cm^{-1}.

rovibrational is mediated by odd changes in both ν_4 and ν_5 or in ν_6, but the total angular momentum and parity are preserved. Throughout this paper we thus label the rotational levels prepared as $J_{K_a K_c}$ according to their identity in S_1. These are the standard asymmetric top quantum numbers: J is the total angular momentum quantum number and K_a and K_c specify the projection of the angular momentum onto the *a*- and *c*- inertial axes, respectively. H_2CO exists as two nuclear spin isomers, *ortho* and *para*, and it has been shown that nuclear spin is preserved into the H_2 product even in the case of roaming reactions.[14] For the S_1 vibrational bands considered here, with odd ν_4 or ν_5/ν_6 but not both, even K_a levels are exclusively *ortho* and odd K_a levels are exclusively *para*. On the ground state this association is reversed.

Photofragment Excitation Spectra

To illustrate the transitions used in the subsequent discussion, we begin by showing photofragment excitation spectra recorded on the $2^1 4^3$ and $2^6 4^1$ bands. We also obtained such spectra for many other bands, and these are in general fully rotationally resolved and assigned. PHOFEX spectra for the $2^1 4^1$, $2^2 4^3$ and $2^1 5^1$ bands are given in Fig. S1. The energies are indicated in Fig. 1 for the origins of all bands we discuss here. For $2^1 4^3$ and $2^6 4^1$ we obtained such spectra monitoring several different CO product rotational levels, sensitive to roaming and t-TS pathways, as well as the H atom representing the radical channel; some of these are included in Fig. 2. On $2^1 4^3$ these showed interesting effects as will be discussed below, while on the $2^6 4^1$ band differences in the excitation spectra could be accounted for by small differences in the molecular beam temperature under which the spectra were obtained.

Following acquisition and assignment of the PHOFEX spectra, a variety of measurements were then made to probe dissociation via specific S_1 H_2CO rovibrational levels. These include CO rotational distributions for many upper state levels as well as VMI studies for a range of product CO rotational levels from this suite of parent rovibrational levels. The latter then yield state-correlated TEDs that are rich in dynamical information.

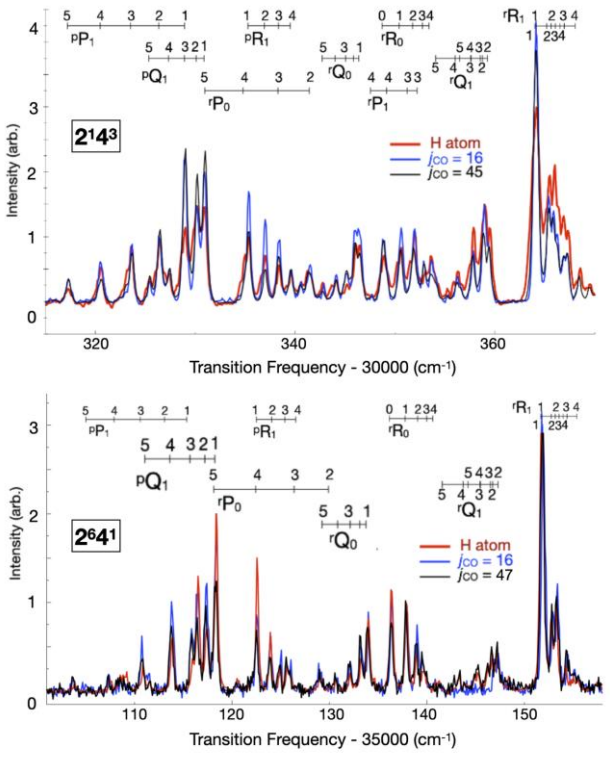

Figure 2. Photofragment excitation (PHOFEX) spectra on the indicated vibrational band in S_1 obtained by monitoring specific CO rotational levels or the H atom product.

Nodal structure in the rotational distributions and TEDs

Here we examine evidence for nodal structure at the t-TS manifested in the rotational distributions both below the roaming threshold and in the presence of roaming and the orbiting resonance we recently identified. We then use the TEDs, obtained from images shown in Fig. S2, to explore this structure and in one case to attempt to dissect the channels coupling S_1 to S_0. Recently, Kable and coworkers revealed analogous features in the roaming region, seen as bimodal CO rotational distributions for specific H_2 product states.[2] These could be associated with turning points in the H-H coordinate and the associated variation in the exit impact parameters. Here we focus on the region of the t-TS using CO measurements which provide the complete product state distributions. Figure 3 shows raw CO rotational spectra following dissociation via a range of parent rotational levels of the 2^14^1 band, 750 cm^{-1} below the radical onset, and of 2^14^3 which is just above it. The former has sufficiently low energy that roaming is absent, while the latter is known to be affected by roaming. These plots show remarkable oscillations in the CO rotational distributions that reflect nodal structure at the t-TS. Here we can examine the nature of this structure using the TEDs and investigate the consequences in the presence of the roaming resonance. Analogous measurements of the rotational distributions for the 2^14^1 band were reported by van Zee, Moore and coworkers using VUV laser-induced fluorescence detection of the CO.[7] Although we report a greater range of levels here with more detailed structure visible, the general features for 2^14^1 are entirely consistent with the observations and analysis reported earlier. That is, the CO rotational distributions typically show broad peaks at high rotational excitation, but the location and width of these peaks change from ~j_{CO}=45 for the excitation to the 0_{00} level to 32 for the 2_{02} level only 6 cm^{-1} higher in energy. Interestingly, preparation of the 1_{11} level gives rise to two distinct peaks of nearly equal magnitude with a minimum near j_{CO}=40; however, van Zee et al. did not show a measurement for this level.[7]

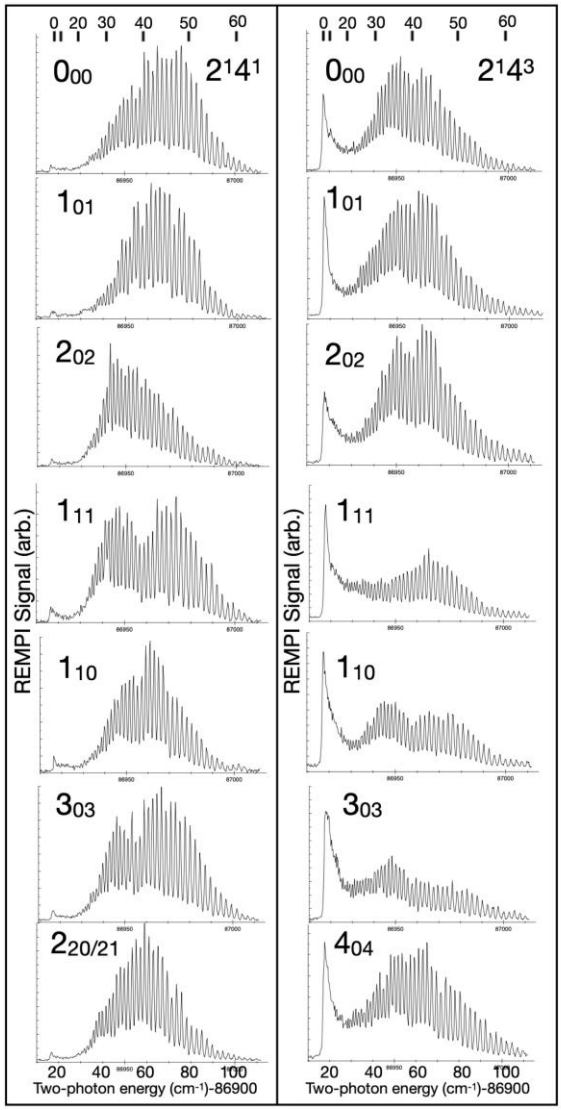

Figure 3. Raw CO (v=0) REMPI spectra obtained below the radical threshold (left) and just above it (right) showing oscillations in the rotational distributions with small changes in excitation energy. The 1_{11}, 1_{10}, and 3_{03} distributions from 2^14^3 show the impact of the orbiting resonance with significant suppression of the high j_{CO} component relative to low j_{CO} roaming (see text).

These profound variations of the CO rotational population with very small changes in total energy in the 2^14^1 band were interpreted to arise from projections of the ergodic, highly excited S_0 rovibrational levels onto the t-TS. This was modelled using random matrix theory to generate the vibrational composition at the t-TS,[6] with the rotational reflection principle then used to project the TS wavefunction to the products. Van Zee et al. suggested that based on the density of states there should be two to five channels coupling S_1 to S_0 for any given parent rotational level. A greater number of coupling channels would obviously tend to blur distributions that might be structured for individual components. The modelling indicated that, as one might expect, a simple Gaussian rotational distribution implied only zero-point vibrational population at the TS. One aspect of the distributions not captured in the modelling – which was based on a harmonic treatment – is asymmetry in the distributions, which is seen very clearly in our measurements. This asymmetry is presumably due to the anharmonicity as well as the different anisotropies of the PES for dissociation from the corresponding turning points. A symmetric bifurcation such as that seen in our 1_{11} level was clearly reproduced in their simulations when two channels, one sharply peaked (zero point) and one v=1 level were combined in phase.

Figure 3 shows what happens when roaming is introduced in the 2^14^3 excitation. For the lowest levels we find broad gaussian shaped distributions that have a consistent "notch" which is also seen in some of the 2^64^1 results (*vide infra*). In all cases we have a substantial contribution at low j_{CO} from roaming as expected. However, on three levels shown, 1_{11}, 1_{10} and 3_{03}, there is a substantial reduction of the high-j_{CO} component and a corresponding enhancement of the low j_{CO} roaming, with the latter identification confirmed by imaging measurements. We found up to a factor of two enhancement in the roaming yield on 3_{03} relative to 2_{02} and this enhancement

was seen on a number of levels all within 20 cm^{-1} below the H+HCO(K_a=1) threshold.[4] We suspected a role for out-of-plane motion in the enhanced roaming and examined this using QCT calculations in which, in one case, all momenta were confined to the plane.[4] The planar trajectories showed reduced roaming and enhanced high j_{CO} products, consistent with the notion that roaming preferentially involves out-of-plane motion as suggested by the roaming saddle point first identified by Harding and coworkers.[41] The suggestion of the appearance of an orbiting resonance associated with HCO(K_a =1) was supported by quantum dynamics calculations in reduced dimensionality.[4] These quantum studies showed evidence of resonances at the threshold of the radical channel, and analysis of the wavefunctions showed significantly enhanced out-of-plane motion. We will return to this view of threshold resonances facilitating roaming in our discussion of the $2^6 4^1$ results below.

One question raised by van Zee et al. was the change in energy partitioning as the rotational distributions shift. Detailed TEDs were not available to them, but they did compare relative yields of v=3 and v=1 for H_2(j=4) for dissociation from several parent levels.[7] They found a variation in this ratio of a factor of two and noted that the larger v=3 fraction was associated with lower maxima in the CO rotational distributions. The special significance of this relative yield of higher vibrational levels of H_2(v=3-5) is clearly seen in our TEDs for $2^1 4^3$, and a close examination of these in view of the vibrational modes of the t-TS, shown in Fig. 4A, is very revealing. The lowest frequency mode at t-TS is ν_5, roughly corresponding to HCO bend. Trajectories initiated from the turning points for ν_5 (Table 1) showed the greatest dispersion in the product CO rotation as may be expected. The other TS mode playing an important role in H_2 vibration, in addition to the reaction coordinate itself, is ν_3. Trajectories from the ν_3 turning points did not directly lead to products, so a small momentum was added to the reaction coordinate in that case. As had previously been suggested,[12] the turning points at the zero-point level correspond roughly to H_2(v=3), and there is only modest dispersion in CO rotation. However, with one quantum in ν_3, the outer turning point leads to population approaching H_2(v=5). Moreover, for $1\nu_3$, a large dispersion in the CO rotation is also seen, with high vibrational excitation in H_2 accompanied by low rotational excitation in CO. This suggests the underlying v=3,4 population in H_2 that appears in lower rotational levels of CO (j_{CO}=25-32) may be associated with extended ν_3, while the large H_2(v=0-3) population with is associated with ν_5. It is also instructive to compare the overall rotational distributions for H_2(v=0-2) and H_2(v=3-5), which we have done using QCT (Fig. 4D**)**. The lower vibrational excitation is clearly associated with greater rotational excitation. This can be attributed both to the forces and impact parameter distribution acting at the TS as inferred from Table 1, and to the accumulated exit channel repulsion that will be greater for the vibrationless species. We thus attribute the overall association of high vibrational states of H_2 with low rotation in CO chiefly to ν_3.

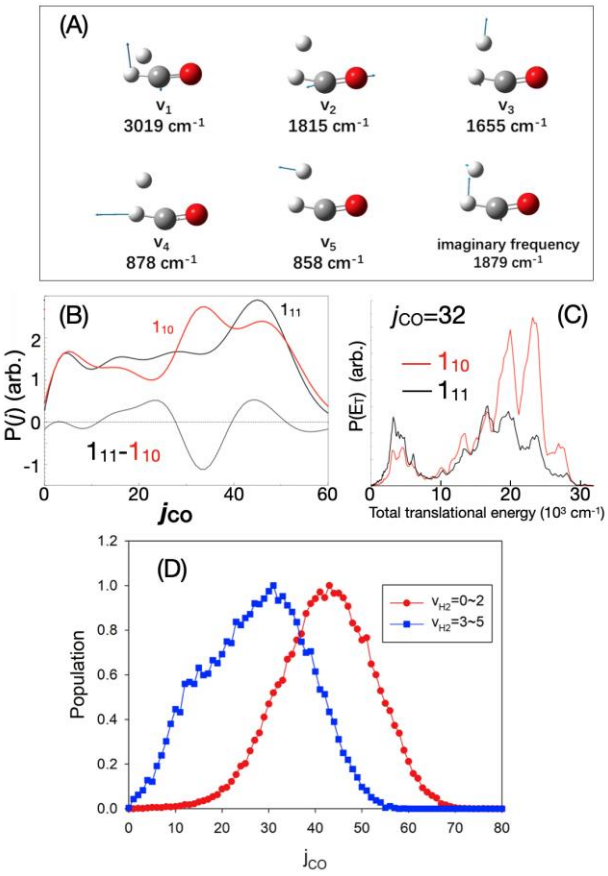

Figure 4. Unravelling correlations between CO rotation and H_2 vibration. A) Vibrational modes of the t-TS. B) CO rotational populations from the indicated parent rotational levels prepared via the $2^1 4^3$ band in S_1, strongly modulated by the resonance. C) TEDs for the two parent rotational levels in (B), scaled by their relative population. D) CO rotational distributions from QCT calculations on $2^1 4^3$ binned according to co-fragment H_2 vibration.

Table 1. *(v,j)* states of H_2 and CO for trajectories starting from turning points at t-TS. For ν_3 small threshold momenta were added along the reaction coordinate. Trajectories from ν_4 returned to the well and did not dissociate.

Turning points	ν_t=0		ν_t=1	
	H_2	CO	H_2	CO
ν_1-inner	v=0; j=11	v=0; j=46	v=2; j=8	v=0; j=41
ν_1-outer	v=2; j=0	v=0; j=41	v=2; j=5	v=0; j=39
ν_2-inner	v=1; j=3	v=4; j=41	v=1; j=2	v=6; j=40
ν_2-outer	v=0; j=1	v=1; j=50	v=0; j=1	v=1; j=53
ν_3-inner	v=3; j=1	v=0; j=37	v=5; j=2	v=0; j=31
ν_3-outer	v=0; j=3	v=1; j=45	v=0; j=1	v=0; j=51
ν_5-inner	v=0; j=7	v=0; j=25	v=0; j=7	v=0; j=23
ν_5-outer	v=0; j=0	v=0; j=50	v=0; j=0	v=1; j=49

We now look in detail at two levels impacted by the resonance we previously identified, 1_{11} and 1_{10} of $2^1 4^3$. Fig. 4B shows the rotational distributions for these after fitting the REMPI spectra and accounting for the line strengths and degeneracy, along with a plot of the difference between them. The greatest difference appears in the region j_{CO}=30-34, where the 1_{11} level has much larger population. In Fig. 4C we show the TEDs for these two levels scaled by the populations from the REMPI measurements. We see the larger population for 1_{11} appears mainly in low vibrational levels of H_2: v=0-3;

alternatively, we can say for the 1_{10} level this low vibrational excitation of H_2 is strongly suppressed. This suggests that large differences in the relative wavefunction amplitudes in ν_3 and ν_5 are likely responsible here, impacted by the resonance that shifts population to roaming. This may involve differences in the out-of-plane mode ν_4 as well.

Another remarkable aspect of the 2^14^3 TEDs is seen in a close examination of the three lowest levels, 0_{00}, 1_{01} and 2_{02}. These are *ortho* levels below the orbiting resonance, and a cursory glance at the rotational distributions in Fig. 2 suggests little difference among them. The TEDs from these three levels are shown for six different product CO rotational states in Fig. 5. In each case, we first plot the distributions separately, while in the second plot we compare the average of 0_{00} and 1_{01} with 2_{02}. This strategy was suggested by the data itself, which seemed to show complementary peak intensities for 0_{00} and 1_{01}. The result of this comparison is quite striking: within experimental uncertainty, the average of the first two matches 2_{02} extremely well for all product states. Dissociation via the 0_{00} level consistently shows greater H_2 vibrational excitation, while 1_{01} shows greater low H_2 vibrational populations. As mentioned above, van Zee et al. had suggested that two to five channels would be expected to couple S_1 to S_0 for 2^14^1 and we expect larger numbers here. However, one way to interpret this result is simply to suggest that 0_{00} and 1_{01} each represent a single channel connecting S_1 to the S_0 TS, and 2_{02} carries both. At first glance this appears unlikely for several reasons. First, one would expect these complex amplitudes to show interference, and there is no sign of this. Second, these levels are spread by 6 cm^{-1} in total energy, which would seem too far to suggest that they possess the same vibrational composition. However, we can bear in mind that this includes differences in overall rotation, and except for the 0_{00} level, the rovibrational character can be altered through Coriolis coupling. Although Coriolis coupling can mix all levels in general, for these low rotational levels such mixing is not likely to be complete. At this point we must concede that the results in Fig. 5 are provocative but lacking a definitive explanation.

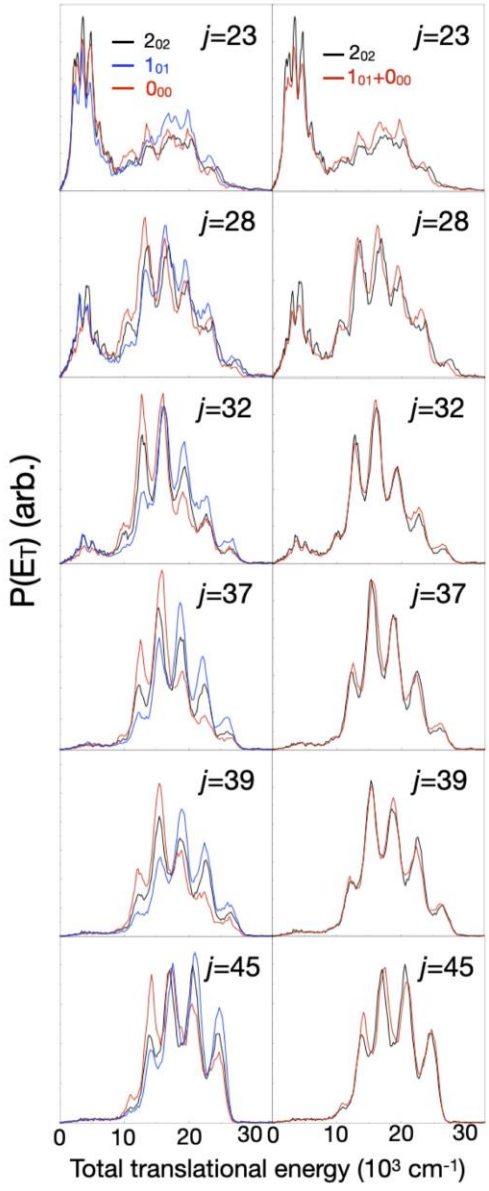

Figure 5. Translational energy distributions for the indicated CO (v=0) level following excitation of 0_{00}, 1_{01} and 2_{02} on the 2^14^3 band (left). Right column shows 2_{02} compared to the average of 0_{00} and 1_{01}.

Roaming dynamics on the 2^64^1 band

We now turn to an examination of the 2^64^1 band which is 5000 cm^{-1} above the radical onset. This is one of many bands studied by Kable and coworkers in an exhaustive investigation of formaldehyde dissociation dynamics from the roaming threshold to above the three-body dissociation limit.[15, 34] Interestingly, significant roaming was observed well above that limit. Kable and coworkers reported results for the strong $2_{20}/2_{21}$ transition 46 cm^{-1} above the band origin using 2D REMPI, while we here study several of the lowest rotational levels and report total TEDs for j_{CO}=28.

In Fig. 6A we contrast results from 1_{01} (*ortho*) and 1_{10} (*para*) excited state preparation. It is immediately apparent that these levels both show a great deal of high vibrational population of H_2 that we associate with roaming, but there are some obvious differences. The differences here arise from the change in the total energy as well as the different grids of product levels available for *para* and *ortho* formaldehyde given that they dissociate exclusively to even or odd rotational levels of H_2, respectively. In Fig. 6B, we focus on the *ortho* levels in which we find a striking effect: increasing the parent rotational energy gives rise to a monotonic increase in the roaming yield (here defined as the fraction of molecular products giving H_2 $v \geq 6$) up to the 4_{04} level, which then decreases to $2_{20}/2_{21}$. Furthermore, it appears mainly to result from a change in the $H_2(v=8)$ population. To demonstrate this, we show fits (Fig. 6C) of these distributions in which individual vibrational contributions are modelled as gaussians with an appropriate centre and width. The v=8 contribution is highlighted and plotted in Fig. 6D. It grows from a contribution of 7% for the 0_{00} level to 12% for the 4_{04} level. The total roaming yield on j_{CO}=28 here similarly grows from 50% for the 0_{00} level to 61% on the 4_{04} level. The *para*

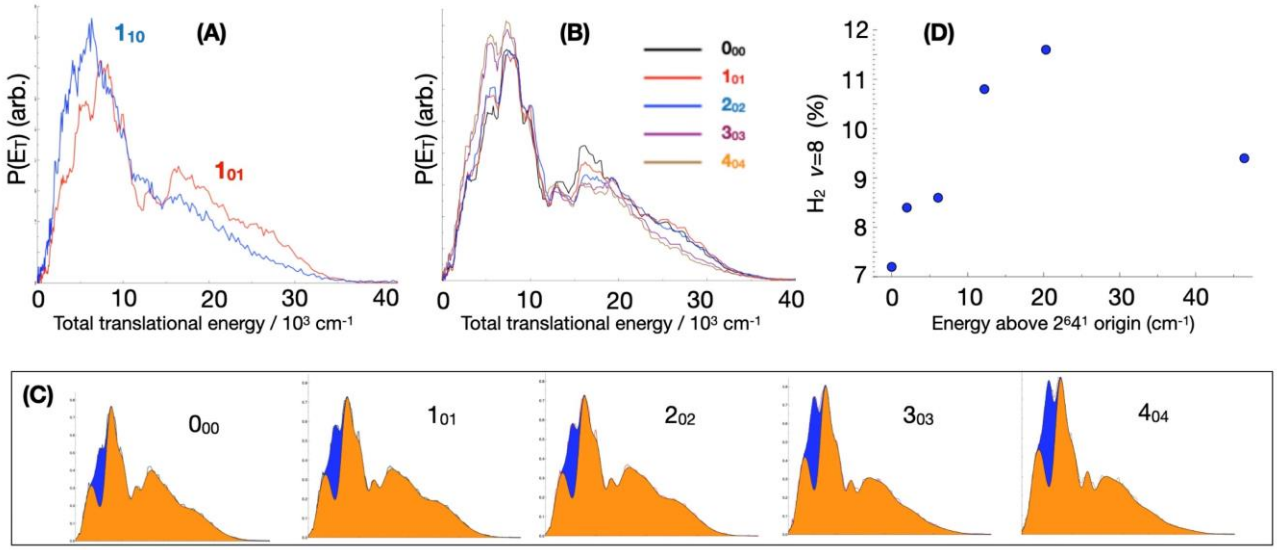

Figure 6. Results for j_{CO}=28 TEDs following $2^6 4^1$ excitation. A) Comparison of 1_{10} (*para*) with 1_{01} (*ortho*) excitation. B) Dependence of *ortho* TEDs on parent rotational level. C) Fits highlighting H_2(v=8) contribution. D) H_2(v=8) contribution vs. energy.

levels 1_{10} and 1_{11}, located at 9.4 cm^{-1} above the origin (between 3_{03} and 4_{04}), also show greatly enhanced H_2(*v*=8) and a roaming yield of 60%, but because of the different H_2 rotational levels involved it is difficult to isolate the *v*=8 level for a close comparison with the *ortho* levels. Product branching and roaming yields are compiled in Table 2 from QCT calculations and experiment.

There are two remarkable aspects of these $2^6 4^1$ observations. One is the obvious change in the TEDs with small changes in energy. We have not seen this phenomenon on other bands except on the $2^1 4^3$ level where we identified the resonances discussed above. These effects are also not seen in QCT simulations, suggesting a possible quantum origin. The other remarkable feature is the sheer magnitude of the roaming contribution here, up to ~60% of the products for j_{CO}=28 is associated with product states we would usually attribute to roaming. One could argue that some substantial fraction of the H_2($v \geq 6$) is now associated with the t-TS pathway, but this difficult to rationalize in light of the discussion above of the H-H bond distances at the turning points for the TS, as well as the clear break in the distribution with the dramatic increase on the low translational energy side occurs just where the roaming contribution is expected.

We considered several different possibilities to account for the large roaming yield seen here. One was based on the recognition that this level is near in energy to the MEX of the S_1 and S_0 PESs. The $2^6 4^1$ energy is slightly below the barrier separating the Franck-Condon region on S_1 from the MEX,[18, 19] but tunnelling through that barrier could lead the system to a region where direct coupling and distinct dynamics might take place as originally suggested by Robb and coworkers.[22] Trajectories were initiated from the MEX with momenta randomly sampled either from both the ***g***- and ***h***-vectors, or from the ***g***-vector alone. The results, shown in Table 2, show that trajectories begun from the MEX show significantly reduced roaming overall but oddly it is relatively enhanced for product levels j_{CO}=26-30. Sampling from ***g***- and ***h***-vectors or ***g***-vector alone had a significant impact on the branching to the radical channel, with the former attenuating the radical yield and the latter enhancing it with respect to trajectories from the S_0 minimum. It is known that the MEX is higher in energy than t-TS and the roaming transition state (r-TS) with a structure in between,[42, 43] but the internal conversion is a complicated nonadiabatic problem and the trajectories might emerge on the S_0 state far away from the MEX.[44] It is interesting to consider that the roaming yield on j_{CO}=28 might specifically be enhanced

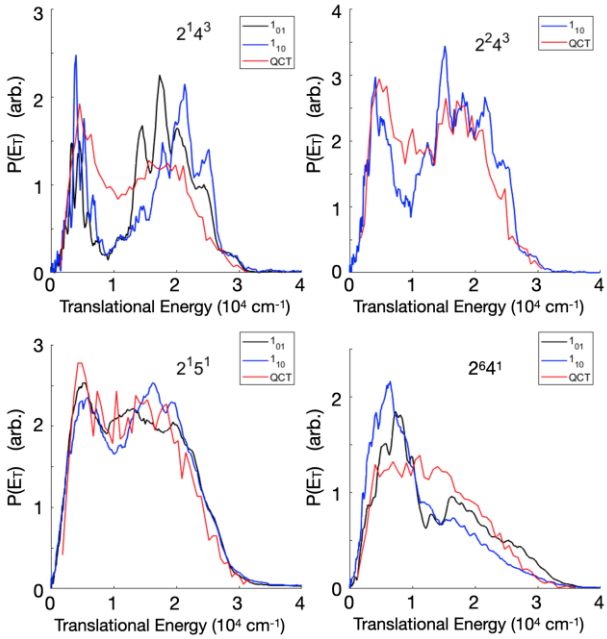

Figure 7. QCT results for j_{CO}=28 compared to experimental measurements following excitation of indicated rotational levels in S_1 for selected vibrational bands.

by a mechanism that populates unusual roaming levels while reducing the overall roaming yield.

Although this view affords some grounds for speculation, an alternative mechanism with parallels to the 2^14^3 case provides a more compelling explanation. In Fig. 1 we showed the bands we have examined in H_2CO along with the corresponding near-coincident thresholds for H+HCO. As noted in the introduction, the 2^14^3 and 2^64^1 origins are 12 and 15 cm^{-1} above the H+HCO (0,0,0) and (0,2,1) thresholds, respectively. Origins for the other bands we have so far examined are >100 cm^{-1} above the corresponding thresholds. For roaming to occur in this case, the system must have at least this much energy provided by the H-HCO interaction: the system cannot roam that far and long-lived roaming resonances are unlikely. The fact that the roaming contribution on j_{CO}=28 declines as the energy is further increased to the $2_{21}/2_{20}$ level also argues against the MEX mechanism and in favour of the resonance effects.

Table 2. Product branching (%) from QCT calculations or experiment where indicated. For MEX-1 momenta were randomly sampled from ***g***- and ***h***-vectors while for MEX-2, only the ***g***-vector. Roaming yield is defined as the fraction of the total H_2+CO product giving $H_2(v \geq 6)$.

	2^14^3	2^24^3	2^15^1	2^64^1	2^64^1-MEX1	2^64^1-MEX2
QCT (H_2+CO)	44.5	43.8	43.1	44.6	60.0	36.5
QCT (H+HCO)	55.8	56.2	56.9	55.4	40.0	63.6
QCT (roam)	12.4	12.9	15.2	21.6	13.6	13.7
Expt (roam)	18-35[a]	22[c]	-	21[b]	-	-
QCT (j_{CO}=26-30)	14	13	16	21	21	36
expt (j_{CO}=28)	15-36	21[c]	28[c]	50-61[c]		

[a]ref. 4

[b]ref. 34

[c]This work

Further evidence then in support of the role for the HCO(0,2,1) threshold is seen in Fig. 7 in which we show TEDs for j_{CO}=28 we have obtained on four different bands along with analogous QCT results for j_{CO}=27-29 for comparison. The distributions for 2^14^3 vary significantly and disagree with the trajectory results as also seen in Fig. 5. The intermediate 2^15^1 and 2^24^3 TEDs show better agreement. The 2^64^1 TED shows the largest discrepancy with the roaming contribution strongly underestimated in the trajectory data. This is also seen in Table 2 in which we compare the experimental j_{CO}=28 roaming fraction with the corresponding value from QCT, along with the total roaming yield determined by QCT. At present we have only limited data for the higher bands and cannot compare our total roaming yield except on 2^14^3. Our direct fits of the $H_2(v\geq6)$ yield for j_{CO}=28 modestly exceed the corresponding trajectory results but this may be a result of different binning. The anomalous behaviour of 2^14^3 and 2^64^1 stand out regardless.

Kable and coworkers reported values for the roaming fraction on a number of bands including 2^64^1.[34] Their values were consistently in the range of 15-20% except for the 2^44^1 level which was only 8%. Their analysis involved separate measurements of j_{CO}=40 and 10 to determine the nature of the t-TS and roaming contributions, and this was then used to determine the overall branching. One aspect of the j_{CO}=40 distributions they reported is, at lower excitation energy, bimodality attributed to the t-TS pathway that leads to assignment of some of the low translational energy products to the t-TS channel. On the 2^64^1 band these distributions are overlapped and they note it is not possible to disentangle them. On the j_{CO}=28 products as we have shown, we can fit the distributions directly in the presence of this significant roaming and we do not see evidence of this contribution. If present, it will be a smaller relative contribution on j_{CO}=28. In any case, we do not have the complete data on the higher bands for a determination of the overall roaming yield, so a direct comparison to the Kable results is not possible.

A related issue regarding roaming yield concerns the QCT results. Although previous experimental results reported roaming yields of 16 to 21% typically[34] and as we saw up to 35% on the 2^14^3 resonance,[4] the previous QCT results reported much lower roaming, typically around 12%, and a much lower radical yield as well.[15] As shown in Table 2, calculations on the new PES from Houston and Bowman,[17] also used here, show much larger roaming overall and considerably larger radical yield for the 2^14^3 band. This is probably because the t-TS in the previous PES[16] was considerably looser than in the newer surface so that dissociation via the t-TS was strongly favoured at threshold.

Our results suggest an impact on roaming yield when new product channels emerge in HCO at energies just below bands in the H_2CO $\tilde{A}$ state spectrum. There are 15 bound vibrational levels of $HCO(X^2A')$[45] and a few exhibit near-coincidences with $H_2CO(S_1)$ vibrational bands. We predict a significant impact on the roaming fraction and, as we saw on 2^14^3, possible impact on the t-TS and radical yields as well when these $\tilde{A}$ state vibrational bands are excited at energies near the HCO thresholds. One interesting thing to note is that these studies have largely been conducted in cold molecular beams, but the first observation of the low j_{CO} products we associate with roaming was on the 2^34^1 band in a room temperature cell.[46] A large contribution was reported at room temperature, but found to be much lower when that band was excited in a cold molecular beam.[8] We estimate the 2^34^1 band is ~400 cm^{-1} above the (0,0,1) level of HCO so it seems unlikely – but not impossible – that parent rotational excitation could play a role in bringing these vibrational levels into resonance. Alternatively, hot band excitation may have played a role, as the room temperature spectra were not prepared via known lines owing to spectral congestion. In any case it is useful to remember that these effects, seen here in beams at ~5 K, may have a different manifestation in other conditions of interest such as the troposphere. What is clear is from this work is that resonances may profoundly impact the dynamics even at these high energies when there is a low-density component of the phase space – the roaming region – that is only weakly coupled to the high-density, strongly interacting region.

Conclusions

Studies of formaldehyde dissociation dynamics following excitation in the vicinity of the radical threshold and 5000 cm^{-1}

above it showed several unusual features providing new understanding into quantum aspects of its unimolecular decomposition. Variations in the product CO rotational distributions with small changes in excitation energy were used in conjunction with total TEDs and QCT calculations to gain insight into the vibrational structure at the t-TS and to highlight a roaming resonance recently identified that we associate with the threshold for H+HCO(0,0,0). Enhanced roaming on the $2^6 4^1$ band that is not reproduced by the QCT calculations is attributed to a similar resonance leading to H+HCO(0,2,1). Other near coincidences between S_1 levels and H+HCO thresholds are thus predicted to show interesting, related behaviour.

Author Contributions

CDF: Investigation (experiment), Analysis, Writing-Reviewing and Editing; **CX**: Investigation (theory), Analysis, Writing-Reviewing and Editing; **HG**: Conceptualization, Supervision, Writing – Reviewing and Editing; **AGS**: Conceptualization, Supervision, Analysis, Writing-Original draft.

Conflicts of interest

There are no conflicts to declare.

Acknowledgements

This work is funded by a MURI grant from the Army Research Office (W911NF-19-1-0283 to H.G. and A.G.S.) and by the National Natural Science Foundation of China (Grant No 22073073 to C.X.).

Notes and references

1. C. B. Moore and J. C. Weisshaar, *Annu. Rev. Phys. Chem.*, 1983, **34**, 525-555.
2. M. S. Quinn, K. Nauta, M. J. T. Jordan, J. M. Bowman, P. L. Houston and S. H. Kable, *Science*, 2020, **369**, 1592-1596.
3. T. Endo, S. P. Neville, V. Wanie, S. Beaulieu, C. Qu, J. Deschamps, P. Lassonde, B. E. Schmidt, H. Fujise, M. Fushitani, A. Hishikawa, P. L. Houston, J. M. Bowman, M. S. Schuurman, F. Légaré and H. Ibrahim, *Science*, 2020, **370**, 1072-1077.
4. C. D. Foley, C. Xie, H. Guo and A. G. Suits, *Science*, 2021, **374**, 1122-1127.
5. W. F. Polik, D. R. Guyer and C. B. Moore, *J. Chem. Phys.*, 1990, **92**, 3453-3470.
6. W. F. Polik, D. R. Guyer, W. H. Miller and C. B. Moore, *J. Chem. Phys.*, 1990, **92**, 3471-3484.
7. R. D. van Zee, C. D. Pibel, T. J. Butenhoff and C. B. Moore, *J. Chem. Phys.*, 1992, **97**, 3235-3244.
8. R. D. van Zee, M. F. Foltz and C. B. Moore, *J. Chem. Phys.*, 1993, **99**, 1664-1673.
9. A. C. Terentis, S. E. Waugh, G. F. Metha and S. H. Kable, *J. Chem. Phys.*, 1998, **108**, 3187-3198.
10. H.-M. Yin, K. Nauta and S. H. Kable, *J. Chem. Phys.*, 2005, **122**, 194312.
11. D. Townsend, S. A. Lahankar, S. K. Lee, S. D. Chambreau, A. G. Suits, X. Zhang, J. Rheinecker, L. B. Harding and J. M. Bowman, *Science*, 2004, **306**, 1158-1161.
12. S. A. Lahankar, S. D. Chambreau, D. Townsend, F. Suits, J. D. Farnum, X. Zhang, J. M. Bowman and A. G. Suits, *J. Chem. Phys.*, 2006, **125**, 044303.
13. S. A. Lahankar, S. D. Chambreau, X. Zhang, J. M. Bowman and A. G. Suits, *J. Chem. Phys.*, 2007, **126**, 044314.
14. S. A. Lahankar, V. Goncharov, F. Suits, J. D. Farnum, J. M. Bowman and A. G. Suits, *Chem. Phys.*, 2008, **347**, 288-299.
15. P. L. Houston, X. Wang, A. Ghosh, J. M. Bowman, M. S. Quinn and S. H. Kable, *J. Chem. Phys.*, 2017, **147**, 013936.
16. X. Zhang, S. Zou, L. B. Harding and J. M. Bowman, *J. Phys. Chem. A*, 2004, **108**, 8980-8986.
17. X. Wang, L. Houston Paul and M. Bowman Joel, *Phil. Trans. Royal Soc. A*, 2017, **375**, 20160194.
18. Y. Guan, C. Xie, H. Guo and D. R. Yarkony, *J. Phys. Chem. A*, 2020, **124**, 10132-10142.
19. Y. Guan, C. Xie, H. Guo and D. R. Yarkony, *J. Chem. Theo. Comput.*, 2021, **17**, 4157-4168.
20. J. D. Farnum, X. Zhang and J. M. Bowman, *J. Chem. Phys.*, 2007, **126**, 134305.
21. P. L. Houston, R. Conte and J. M. Bowman, *J. Phys. Chem. A*, 2016, **120**, 5103-5114.
22. M. Araujo, B. Lasorne, M. J. Bearpark and M. A. Robb, *J. Phys. Chem. A*, 2008, **112**, 7489-7491.
23. M. Araújo, B. Lasorne, A. L. Magalhães, G. A. Worth, M. J. Bearpark and M. A. Robb, *J. Chem. Phys.*, 2009, **131**, 144301.
24. M. Araújo, B. Lasorne, A. L. Magalhães, M. J. Bearpark and M. A. Robb, *J. Phys. Chem. A*, 2010, **114**, 12016-12020.
25. A. G. Suits, *Acc. Chem. Res.*, 2008, **41**, 873-881.
26. J. M. Bowman and B. C. Shepler, *Annu. Rev. Phys. Chem.*, 2011, **62**, 531-553.
27. A. G. Suits, *Annu. Rev. Phys. Chem.*, 2020, **71**, 77-100.
28. S. J. Klippenstein, Y. Georgievskii and L. B. Harding, *J. Phys. Chem. A*, 2011, **115**, 14370-14381.
29. D. U. Andrews, S. H. Kable and M. J. T. Jordan, *J. Phys. Chem. A*, 2013, **117**, 7631-7642.
30. J. M. Bowman and P. L. Houston, *Chem. Soc. Rev.*, 2017, **46**, 7615-7624.
31. F. A. L. Mauguière, P. Collins, Z. C. Kramer, B. K. Carpenter, G. S. Ezra, S. C. Farantos and S. Wiggins, *Annu. Rev. Phys. Chem.*, 2017, **68**, 499-524.
32. A. Li, J. Li and H. Guo, *J. Phys. Chem. A*, 2013, **117**, 5052-5060.
33. R. Spence and W. Wild, *J. Chem. Soc.*, 1935, 338-340.
34. M. S. Quinn, D. U. Andrews, K. Nauta, M. J. T. Jordan and S. H. Kable, *J. Chem. Phys.*, 2017, **147**, 013935.
35. C. M. Western, *J. Quant. Spectrosc. Rad. Transf.*, 2017, **186**, 221-242.
36. D. Townsend, M. P. Minitti and A. G. Suits, *Rev. Sci. Instrum.*, 2003, **74**, 2530-2539.
37. D. W. Chandler and P. L. Houston, *J. Chem. Phys.*, 1987, **87**, 1445-1446.
38. A. T. J. B. Eppink and D. H. Parker, *Rev. Sci. Instrum.*, 1997, **68**, 3477-3484.
39. X. Hu, W. L. Hase and T. Pirraglia, *J. Comput. Chem.*, 1991, **12**, 1014-1024
40. V. A. Job, V. Sethuraman and K. K. Innes, *J. Mole. Spectrosc.*, 1969, **30**, 365-426.

41. L. B. Harding, S. J. Klippenstein and A. W. Jasper, *Phys. Chem. Chem. Phys.*, 2007, **9**, 4055-4070.
42. B. C. Shepler, Y. Han and J. M. Bowman, *J. Phys. Chem. Lett.*, 2011, **2**, 834-838.
43. L. B. Harding, S. J. Klippenstein and A. W. Jasper, *J. Phys. Chem. A*, 2012, **116**, 6967-6982.
44. B. Fu, B. C. Shepler and J. M. Bowman, *J. Am. Chem. Soc.*, 2011, **133**, 7957-7968.
45. J. D. Tobiason, J. R. Dunlop and E. A. Rohlfing, *J. Chem. Phys.*, 1995, **103**, 1448-1469.
46. M. F. Foltz, PhD thesis, University of California Berkeley, 1989.